Vol 7, Issue 1, 2024 **Impact Factor: 5.355** DOI: https://doi.org/10.31426/ijamsr.2024.7.1.7017

IJAMSR

International Journal of Advanced Multidisciplinary Scientific Research (IJAMSR) ISSN:2581-4281

"Analysis of a Thermal Energy Storage System for High-Temperature Latent Heat"

Bijaya Kumar Martha [1]

Research Scholar, Department of M. Tech Thermal Engineering,
Sri Satya Sai University of Technology and Medical Sciences, Bhopal, M.P, India.

Dr Sachin Baraskar [2]

Research Guide, Department of M. Tech Thermal Engineering,
Sri Satya Sai University of Technology and Medical Sciences, Bhopal, M.P, India.

ABSTRACT

This study investigates a high-temperature latent heat thermal energy storage (LHTES) system using hydroquinone as the phase change material (PCM) and Therminol VP-1 as the heat transfer fluid (HTF). ANSYS FLUENT simulations, validated by experiments, analyze the impact of pipe geometry, HTF inlet temperature, and flow rate on thermal efficiency and entropy generation, keeping PCM volume constant. Results show lower flow rates improve efficiency and reduce entropy due to decreased viscous dissipation. Higher volume ratios enhance energy efficiency but affect entropy generation depending on flow velocity, while lower HTF inlet temperatures reduce both efficiency and entropy. Volume ratio significantly influences PCM melting time, highlighting the need for a balanced design approach that considers both thermodynamic performance and operational feasibility. This work contributes to the understanding of high-temperature LHTES systems and informs future research incorporating thermo-chemical energy storage.

Keywords: *High-Temperature Thermal Energy Storage (HT-TES), Latent Heat Storage, Thermo-Chemical Energy Storage, Phase Change Material (PCM), Entropy Generation, ANSYS FLUENT, Hydroquinone, Heat Transfer Fluid (HTF), Volume Ratio, Energy Efficiency, Viscous Dissipation.*

IJAMSR

International Journal of
Advanced Multidisciplinary Scientific Research (IJAMSR) ISSN:2581-4281

1. INTRODUCTION

High-temperature thermal energy storage (HT-TES) is crucial for balancing energy supply and demand, particularly in renewable systems. It is utilized in space heating, industrial processes, and solar power generation. HT-TES involves storing thermal energy via heating or cooling a material for later use, enhancing reliability, efficiency, and reducing costs and fossil fuel dependence.

HT-TES systems include sensible heat (STES), latent heat (LHTES), and thermochemical storage. LHTES operates during phase changes of storage materials, offering higher energy density and simplified heat exchange due to near-constant temperatures. Key characteristics of phase change materials (PCMs) include high heat of fusion, good thermal conductivity, and stability.

Recent studies have tested LHTES systems, such as a pilot plant in Spain, revealing that d-mannitol outperforms hydroquinone in energy storage. Various designs have been explored to improve thermal conductivity. Numerical modeling is increasingly used to analyze performance, with findings indicating that factors like tube size and inlet temperature significantly affect charging and discharging times.

Energy and exergy analyses are vital for optimizing TES systems, highlighting the importance of entropy generation. Recent research has demonstrated that optimized designs can reduce solidification times and improve exergy efficiency.

This study introduces a 3D computer model of a high-temperature LHTES system, examining how HTF inlet temperature, volumetric flow rate, and the volume ratio of PCM to HTF influence energy efficiency and entropy generation. Using ANSYS Fluent for simulations, results align well with experimental data, providing new insights into optimizing HT-TES system performance.

2. MATHEMATICAL REPRESENTATION

A computational model has been created using ANSYS FLUENT to simulate the storage of thermal energy within a medium based on molten salt to investigate high-temperature thermal energy storage systems. The design is similar to a shell-and-tube heat exchanger, but to keep simulation time and computational resources to a minimum, only a quarter of the pipe domain is modeled. The phase change material (PCM) chosen for the latent heat storage component is hydroquinone because of its desirable thermal properties, specifically its high latent heat of fusion and suitable melting point. A synthetic heat transfer fluid (HTF) called Therminol VP1 is used to help with thermal energy exchange, and the structural material that separates the PCM and HTF parts is stainless steel. The simulation material properties are listed in Table 1.

IJAMSR

International Journal of
Advanced Multidisciplinary Scientific Research (IJAMSR) ISSN:2581-4281

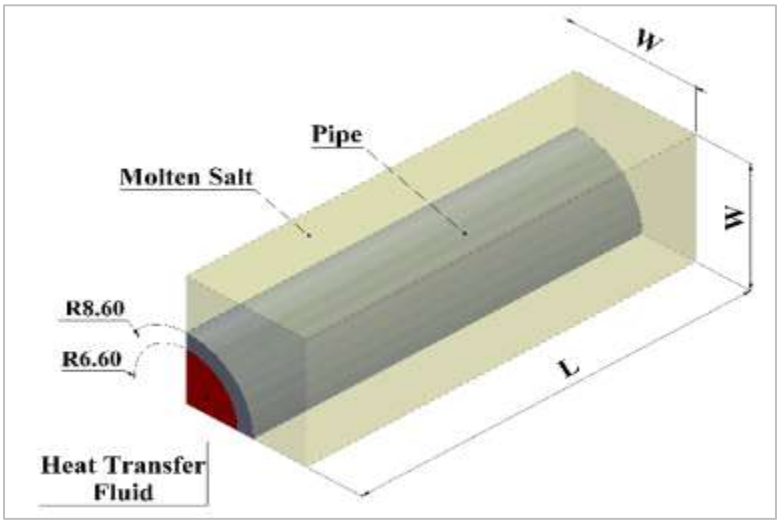

Figure 1: Abridged Three-D Model

Table 1: Three-D Mode Simplified

Properties	Hydroquinone [PCM] [8]	Therminol VP-1 @ 473 K [HTF] [10]	Stainless Steel
Density (kg/m³)	1180	913	8030
Specific Heat (J/kgK)	2500	2048	502
Thermal Conductivity (W/mK)	0.1	0.1138	16.27
Melting Temperature (°C)	168–173	N/A	N/A
Melting Enthalpy (kJ/kg)	205.8	N/A	N/A
Viscosity (mPas)	0.97	0.395	N/A

The two main modes of operation that are examined are the charging and discharging processes. The former involves the transfer of thermal energy from the HTF to the PCM, and the latter involves the reverse flow of stored heat from the PCM to the HTF. These steps mimic the normal cycle of a system that stores latent heat energy. Thermodynamic efficiency and heat transfer performance can be studied by keeping the pipe diameters at 6.6 mm and 8.6 mm, respectively, and keeping the PCM volume constant at 236 ml (236,800 mm³). To make a meaningful comparison with the existing literature, it is necessary to fix the PCM volume [8, cite: 1]. To test its effect on system behavior, the volume ratio of PCM to HTF is varied from 1.5 to 30. Table 2 and Figure 1 display detailed information about the geometric configurations, including volume ratio, pipe length (L), and width (W), for each simulation case.

2.1 Governing Equations

To accurately model the high-temperature thermal energy storage (HTTES) systems employing latent heat and thermo-chemical heat storage mechanisms, the fundamental conservation equations—mass, momentum, and energy—must be resolved within a transient framework. This study assumes constant thermophysical characteristics for all materials involved (as outlined in Table 1), and

IJAMSR

International Journal of Advanced Multidisciplinary Scientific Research (IJAMSR) ISSN:2581-4281

disregards both radiation effects and gravitational forces due to their negligible influence at the considered scales. The energy balance for the heat transfer fluid (HTF), which facilitates thermal exchange within the storage system, is represented by:

$$\rho_{HTF}\frac{Dh_{HTF}}{Dt} = \frac{Dp}{Dt} + k_{HTF}\nabla^2 T + \Phi \tag{1}$$

Here, Φ signifies the viscous dissipation term, which arises due to internal shear within the HTF, expressed as:

$$\Phi = \mu\left(2\left(\frac{\partial u}{\partial x}\right)^2 + 2\left(\frac{\partial v}{\partial y}\right)^2 + 2\left(\frac{\partial w}{\partial z}\right)^2 + \left(\frac{\partial v}{\partial x} + \frac{\partial u}{\partial y}\right)^2 + \left(\frac{\partial w}{\partial y} + \frac{\partial v}{\partial z}\right)^2 + \left(\frac{\partial u}{\partial z} + \frac{\partial w}{\partial x}\right)^2\right) \tag{2}$$

The governing equations for mass and momentum conservation in the HTF are:

$$\nabla \cdot \vec{V} = 0 \tag{3}$$

$$\rho_{HTF}\frac{D\vec{V}}{Dt} = -\nabla p + \mu\nabla^2\vec{V} \tag{4}$$

For the containment material (e.g., the pipe walls) and the phase change material (PCM), the respective energy equations are formulated as follows under the assumption of no internal heat generation:

$$\rho_{pipe}\frac{Dh_{pipe}}{Dt} = k_{pipe}\nabla^2 T \tag{5}$$

$$\rho_{PCM}\frac{DH_{PCM}}{Dt} = k_{PCM}\nabla^2 T \tag{6}$$

In latent heat-based thermal storage systems, where phase transitions play a critical role, the enthalpy–porosity technique is adopted to capture the melting and solidification phenomena. This approach treats enthalpy as the primary variable instead of temperature. The total enthalpy of the PCM is represented as:

$$H_{PCM} = h + H_L \tag{7}$$

where h_{ref} denotes the enthalpy at a reference temperature, and Cp is the specific heat capacity.
The latent heat component H_L is computed based on the liquid fraction ϕ, as follows:

$$H_L = \phi L \tag{9}$$

I J A M S R

International Journal of
Advanced Multidisciplinary Scientific Research (IJAMSR) ISSN:2581-4281

In the enthalpy–porosity framework, the liquid fraction ϕ\phiϕ evolves based on local temperature and is described by:

$$\phi = \begin{cases} 0 & \text{if } T < T_s \quad \text{(Completely Solid)} \\ 1 & \text{if } T > T_l \quad \text{(Fully Liquid)} \\ \frac{T-T_s}{T_l-T_s} & \text{if } T_s \leq T \leq T_l \quad \text{(Mixed Phase)} \end{cases} \tag{10}$$

2.2 Thermodynamic Evaluation

Thermodynamic evaluations, namely energy and entropy analyses, are crucial in the context of HT-TES for determining the size and location of thermal inefficiencies. This study places an emphasis on viscous dissipation losses and notes that thermal leakage, while important in general, loses some of its significance as the system size grows. The methodologies used to calculate entropy and energy are based on known frameworks from previous studies [21,29, cite: 1], with some adjustments to make them suitable for thermo-chemical storage systems and latent heat [25-28, cite: 1].

2.2.1 Energy Evaluation

Based on the earlier-stated assumptions, the global energy conservation equation during either thermal charging or discharging cycles is expressed as:

Based on the earlier-stated assumptions, the global energy conservation equation during either thermal charging or discharging cycles is expressed as:

$$\Delta E_{\text{sys}} = E_{\text{in}} - E_{\text{out}} = U_{\text{in}} - U_{\text{out}} \tag{11}$$

At any given moment, the net change in stored energy within the system is determined by summing the energy changes in each subsystem—namely, the heat transfer fluid (HTF), the structural components (e.g., pipes), and the phase change or thermo-chemical materials:

$$\Delta E_{\text{sys}} = \Delta E_{\text{HTF}} + \Delta E_{\text{Pipe}} + \Delta E_{\text{PCM}} \tag{12}$$

For the HTF:

$$\Delta E_{\text{HTF}} = m_{\text{HTF}} C_{p,\text{HTF}} (T_{\text{HTF}} - T_{\text{HTF,ini}}) \tag{13}$$

While Equation (13) can be used for manual computation, leveraging simulation tools (e.g., ANSYS Fluent) allows more straightforward tracking of thermal energy exchanges between the HTF, containment structures, and the latent/thermo-chemical storage medium.

$$\Delta E_{\text{Pipe}} = \int_0^t Q_{\text{Pipe}}\, dt \approx \sum_{i=0}^{t} Q_{\text{Pipe},i} \tag{14}$$

$$\Delta E_{\text{PCM}} = \int_0^t Q_{\text{PCM}}\, dt \approx \sum_{i=0}^{t} Q_{\text{PCM},i} \tag{15}$$

IJAMSR

International Journal of Advanced Multidisciplinary Scientific Research (IJAMSR) ISSN:2581-4281

The efficiency of each thermal cycle stage is then assessed. For instance, the efficiency of thermal charging—representing the effectiveness of energy transfer to the storage medium—is defined as:

$$\eta_{\text{ch}} = \frac{E_{\text{des}}}{E_{\text{total}}} = \frac{\Delta E_{\text{sys}}}{U_{\text{in}} - U_{\text{out}} + V(P_{\text{in}} - P_{\text{out}})} \tag{16}$$

Where U, H, V, and P denote internal energy, enthalpy, volume, and pressure, respectively.

For the discharge phase, the efficiency quantifies the usable thermal energy recovered, typically observed as enthalpy gain in the HTF:

$$\eta_{\text{dis}} = \frac{H_{\text{in}} - H_{\text{out}}}{\Delta E_{\text{sys}}} = \frac{U_{\text{in}} - U_{\text{out}} + V(P_{\text{in}} - P_{\text{out}})}{\Delta E_{\text{sys}}} \tag{17}$$

Given that calculated efficiencies frequently exceed 99% due to minimal viscous losses, a normalized or “contracted” efficiency metric is used to better illustrate performance deviations in the last percentile:

$$\eta_{\text{con}} = \frac{\eta - 0.99}{0.0001} \tag{18}$$

2.2.2 Entropy Assessment

In parallel, entropy assessments offer insights into the irreversibilities present in the system. The general entropy balance is given by: In parallel, entropy assessments offer insights into the irreversibilities present in the system. The general entropy balance is given by:

$$\Delta S_{\text{sys}} = S_{\text{in}} - S_{\text{out}} + S_{\text{gen,heat}} \tag{19}$$

The system’s total entropy change is decomposed into contributions from each material domain:

$$\Delta S_{\text{sys}} = \Delta S_{\text{HTF}} + \Delta S_{\text{Pipe}} + \Delta S_{\text{PCM}} \tag{20}$$

For each component:

$$\Delta S_{\text{PCM}} = \frac{\Delta E_{\text{PCM}}}{T_{b,\text{PCM}}} \approx \sum_{i=0}^{t} \frac{Q_{\text{PCM},i}}{T_{b,\text{PCM}}} \tag{21}$$

$$\Delta S_{\text{HTF}} = m_{\text{HTF}} C_{p,\text{HTF}} \ln\left(\frac{T_{b,\text{HTF}}}{T_{\text{ini}}}\right) \tag{22}$$

$$\Delta S_{\text{Pipe}} = m_{\text{Pipe}} C_{p,\text{Pipe}} \ln\left(\frac{T_{b,\text{Pipe}}}{T_{\text{ini}}}\right) \tag{23}$$

Where T_b represents the bulk or average temperature of the respective material.

International Journal of
Advanced Multidisciplinary Scientific Research (IJAMSR) ISSN:2581-4281

The entropy flow associated with the HTF is given by:

$$S_{\text{in}} - S_{\text{out}} = \sum_{i=0}^{t} \dot{m}_{\text{HTF}} C_{p,\text{HTF}} \ln\left(\frac{T_{\text{in}}}{T_{\text{out},i}}\right) \tag{24}$$

Total entropy generation within the system comprises both thermal conduction and viscous dissipation contributions:

$$S_{\text{gen,total}} = S_{\text{gen,heat}} + S_{\text{gen,vd}} \tag{25}$$

Entropy generated from viscous losses is calculated as:

$$S_{\text{gen,vd}} = \frac{V(P_{\text{in}} - P_{\text{out}})}{T_{b,\text{HTF}}} \tag{26}$$

The bulk temperature of the HTF ($T_{b,HTFT}$) can be effectively monitored using commercial simulation tools.

2.3. Boundary Conditions

Figure 2 illustrates the geometry and boundary specifications of the three-dimensional model used in this study. A constant mass flow rate is imposed at the pipe's inlet; however, the volumetric flow rate is treated as a variable parameter. This approach is necessary because the mass flow rate depends on the heat transfer fluid's (HTF) density, which fluctuates with changes in inlet temperature. For this analysis, the volumetric flow rate is varied within the range of 0.3 to 3.8 m^3/h. The inlet temperatures of the HTF—specifically Therminol VP1—are assigned values of either 460 K or 473 K during the thermal charging phase, and 403 K or 418 K during the discharging phase. A pressure outlet condition is defined at the HTF exit, while thermally coupled boundary conditions are applied to the interfaces between the HTF, phase change or thermo-chemical storage media, and the pipe walls.

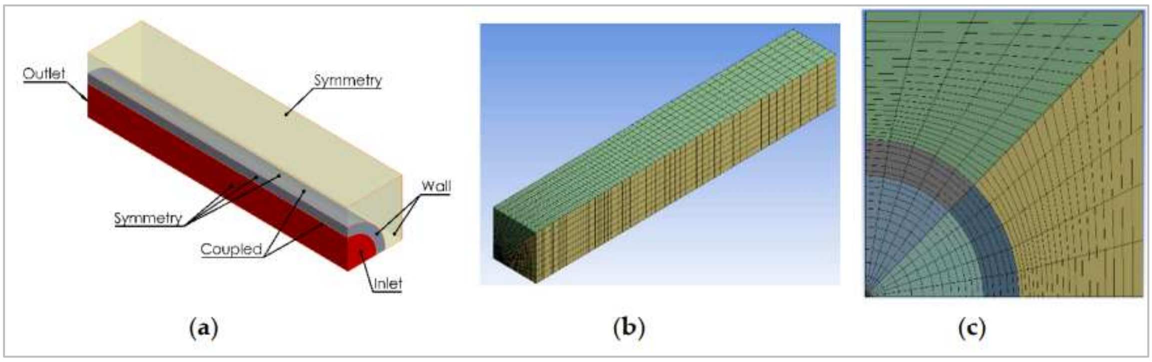

Figure 2: Mesh Generation (a) Boundary Conditions (b) 3D View (c) Front View

Due to symmetrical geometry, only one-quarter of the domain is simulated to reduce computational complexity. The initial temperatures across the HTF, pipe, and storage media domains are specified as either 403 K or 418 K for the charging phase. For the discharging simulation, the final temperature

IJAMSR

International Journal of Advanced Multidisciplinary Scientific Research (IJAMSR) ISSN:2581-4281

obtained from the charging cycle is employed as the initial condition. A comprehensive overview of the simulation parameters is provided in Figure 3.

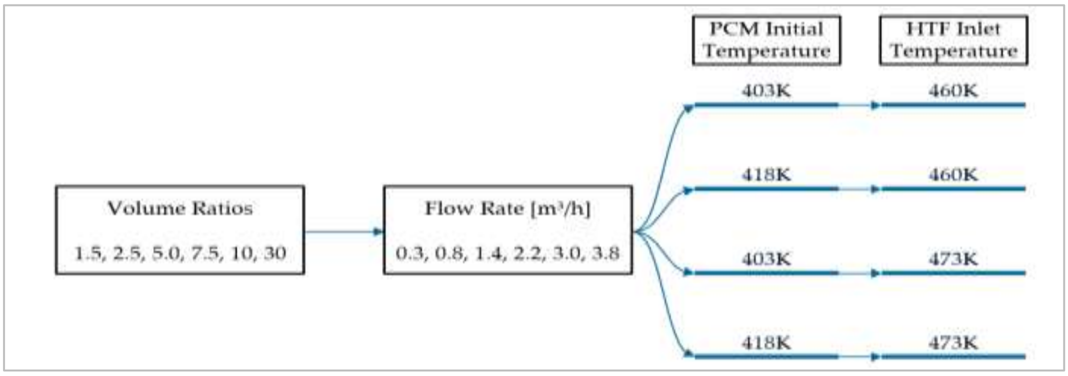

Figure 3: Parametric Simulation Parameters Summarized

3. RESULTS AND DISCUSSION

3.1 Validation of Numerical Model

To ensure the reliability of the simulation results in the context of high-temperature thermal energy storage systems, particularly latent heat and thermo-chemical storage mechanisms, the numerical model was validated against experimental data reported in [8, cite: 1]. The experimental configuration, reproduced schematically in Figure 6, employs a shell-and-tube heat exchanger—tested in two configurations: with and without extended surface fins. For validation purposes, the finless configuration was selected, aligning with the experimental setup for direct comparison.

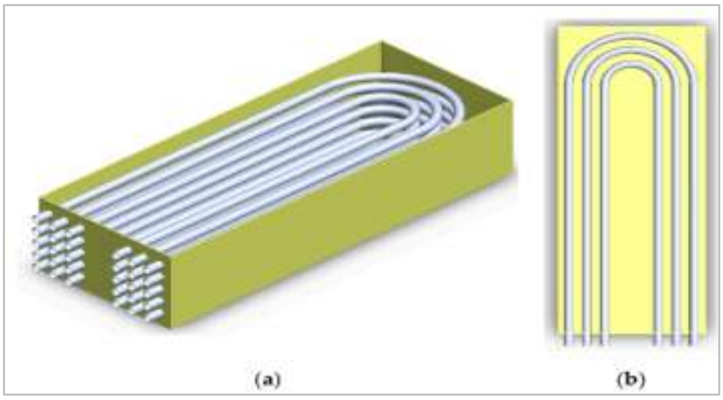

Figure 3: (a) Top View and (b) 3D View of a Shell-And-Tube Heat Exchanger for Low-Hop Transverse Engine Systems (LHTES) Adapted from [8, Cite: 1].

Temperature readings from two of the fifteen sensors, located farthest from the heat exchanger's boundary, served as reference points, correlating with simulated phase change material (PCM) temperatures from the computational mesh. The referenced study included both laminar and turbulent flow conditions, leading to simulations at two volumetric flow rates. For laminar flow, a rate of 1.4 m^3/h ($Re \approx 1633$) was simulated without turbulence modeling, matching original test conditions. Results showed strong agreement with experimental measurements, confirming accurate thermal response predictions.

IJAMSR

International Journal of Advanced Multidisciplinary Scientific Research (IJAMSR) ISSN:2581-4281

In the turbulent regime, a higher flow rate of 3.0 m³/h (Re ≈ 3785) was simulated using the k–SST turbulence model, which effectively predicted complex flow characteristics. Validation for a representative charging case revealed a maximum temperature deviation of 9 K between simulated and observed values, within acceptable error margins. These results demonstrate the model's capability to accurately simulate thermal behavior in latent and thermo-chemical storage systems, providing a solid basis for further performance assessments and design optimizations.

3.2 Thermodynamic Efficiencies

First Law Efficiency

Energy efficiencies are calculated using Equations (11) to (18), with results consistently exceeding 99%. This advantage is due to the systems being treated as adiabatic, where losses mainly occur from viscous heating—these are minor compared to the total stored energy. Although the efficiencies appear high, the impact of viscous heating is examined through the use of contracted energy efficiency (Equation 18), which helps highlight the last percentage of efficiency losses. Without this focused analysis, one might assume the losses are negligible. This is a limitation of conventional energy-based evaluations for latent heat thermal energy storage (LHTES) systems, as they don't consider irreversibilities, which become more significant when storing lower-quality thermal energy.

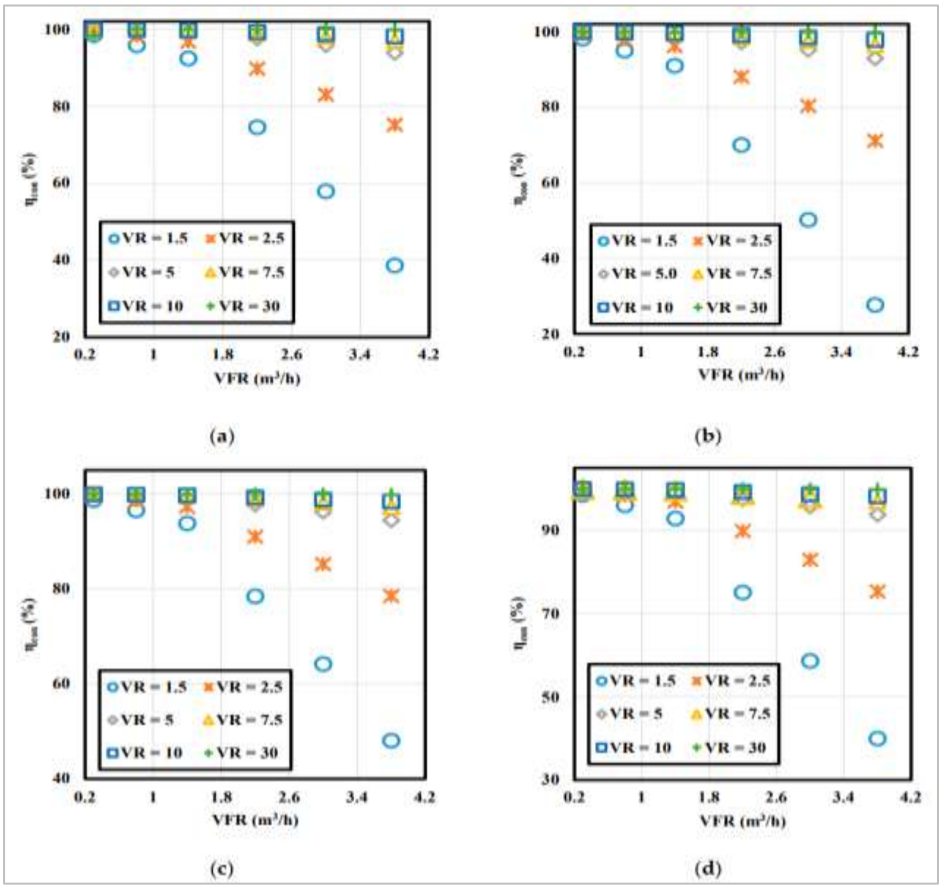

Figure 4: Contracted Energy Efficiencies for Initial PCM-HTF Temperatures Of 403–460 K, 418–460 K, 403–473 K, and 418–473 K for various Volume Ratios (VR) and Volumetric Flow Rates (VFR, in m³/hr).

**International Journal of
Advanced Multidisciplinary Scientific Research (IJAMSR) ISSN:2581-4281**

Figure 7 shows that contracted energy efficiency drops as the flow rate increases, caused by higher fluid velocities leading to more viscous dissipation. The effect of HTF inlet temperature is also shown in Figure 4. Two inlet temperatures and two initial PCM temperatures are tested across varying volume ratios and flow rates. As expected, higher HTF inlet temperatures lead to better efficiencies due to greater temperature differences between the HTF and PCM, resulting in stronger heat transfer, following Newton's Law of Cooling.

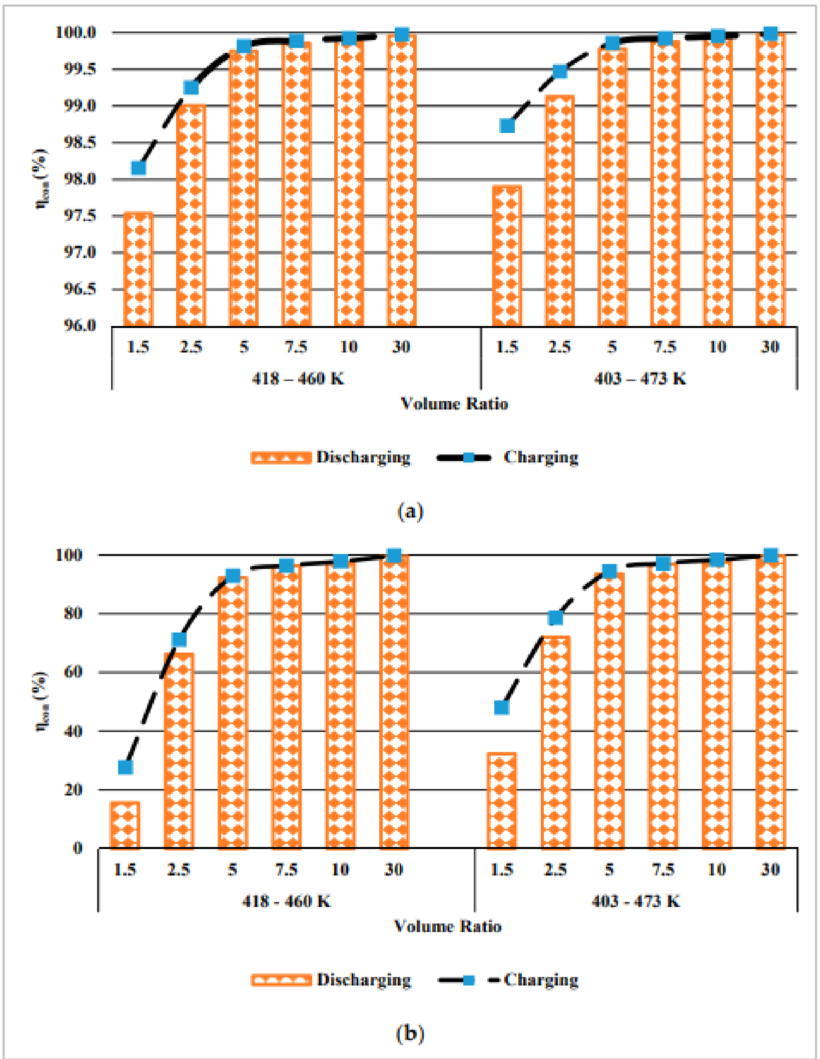

Figure 5: Contracted Energy Efficiency Changes for Charging and Discharging: (a) 0.3 m³/h (b) 3.8 m³/h.

Figure 5 reveals that the influence of volume ratio on contracted efficiency is more noticeable than that of HTF temperature. Since the pipe and tank lengths remain constant, a higher volume ratio leads to a smaller HTF volume and reduced pressure drop, lowering viscous heating. Efficiency improves with higher volume ratios, but this effect depends heavily on flow rate. For example, when the flow rate is 0.3 m³/h, contracted efficiency rises from 98.00% to 99.99% as the volume ratio increases. However, at 3.8 m³/h, it jumps from 26% to 99%. Contracted efficiencies are consistently higher during the charging phase than in discharging, since viscous losses are more significant during discharging.

International Journal of
Advanced Multidisciplinary Scientific Research (IJAMSR) ISSN:2581-4281

4. CONCLUSION

This paper has thoroughly analyzed the performance of a Thermal Energy Storage (TES) system designed for high-temperature latent heat applications. We specifically investigated various aspects crucial for its practical implementation and efficiency, focusing on the material properties, charging/discharging dynamics, and overall system effectiveness. The findings from this analysis provide valuable insights into optimizing such systems for applications requiring efficient heat storage and release at elevated temperatures. The research underscores the potential of high-temperature latent heat TES systems to contribute significantly to energy efficiency and sustainability in various industrial and renewable energy sectors. Further work will explore the long-term cycling stability and cost-effectiveness of these systems under real-world operating conditions.

BIBLIOGRAPHY

1. Farhangi, H. “The Path of the Smart Grid.” IEEE Power and Energy Magazine, vol. 8, no. 1, 2018, pp. 18–28.
2. U.S. Department of Energy Information Administration. Electric Power Monthly. Apr. 2022, www.eia.gov/electricity/monthly/current_year/april2022.pdf. Accessed Jun. 2022.
3. Teleke, S., et al. “Rule-Based Control of Battery Energy Storage for Dispatching Intermittent Renewable Sources.” IEEE Transactions on Sustainable Energy, vol. 1, no. 3, Oct. 2018, pp. 117–124.
4. Dimroth, F., et al. “Wafer Bonded Four-Junction GaInP/GaAs//GaInAsP/GaInAs Concentrator Solar Cells with 44.7% Efficiency.” Progress in Photovoltaics: Research and Applications, vol. 22, no. 3, 2022, pp. 277–282.
5. Li, G., et al. “High-Efficiency Solution Processable Polymer Photovoltaic Cells by Self-Organization of Polymer Blends.” Nature Materials, vol. 4, no. 11, 2019, pp. 864–868.
6. Couture, T., and Y. Gagnon. “An Analysis of Feed-In Tariff Remuneration Models: Implications for Renewable Energy Investment.” Energy Policy, vol. 38, no. 2, 2018, pp. 955–965.
7. Lesser, J. A., and X. Su. “Design of an Economically Efficient Feed-In Tariff Structure for Renewable Energy Development.” Energy Policy, vol. 36, no. 3, 2020, pp. 981–990.
8. Mohammadi, S., S. Soleymani, and B. Mozafari. “Scenario-Based Stochastic Operation Management of Microgrid Including Wind, Photovoltaic, Micro-Turbine, Fuel Cell and Energy Storage Devices.” International Journal of Electrical Power and Energy Systems, vol. 54, Jan. 2022, pp. 525–535.
9. Niknam, T., R. Azizipanah-Abarghooee, and M. R. Narimani. “An Efficient Scenario-Based Stochastic Programming Framework for Multiobjective Optimal Micro-Grid Operation.” Applied Energy, vol. 99, Nov. 2020, pp. 455–470.
10. Hemmati, M., N. Amjady, and M. Ehsan. “System Modeling and Optimization for Islanded Micro-Grid Using Multi-Cross Learning-Based Chaotic Differential Evolution Algorithm.” International Journal of Electrical Power and Energy Systems, vol. 56, Mar. 2020, pp. 349–360.

IJAMSR

International Journal of
Advanced Multidisciplinary Scientific Research (IJAMSR) ISSN:2581-4281

11. Guan, X., Z. Xu, and Q.-S. Jia. "Energy-Efficient Buildings Facilitated by Microgrid." IEEE Transactions on Smart Grid, vol. 1, no. 3, Dec. 2021, pp. 243–252.
12. Hafez, O., and K. Bhattacharya. "Optimal Planning and Design of a Renewable Energy Based Supply System for Microgrids." Renewable Energy, vol. 45, Sep. 2020, pp. 7–15.
13. Dufo-López, R., et al. "Multi-Objective Optimization Minimizing Cost and Life Cycle Emissions of Stand-Alone PV–Wind–Diesel Systems with Batteries Storage." Applied Energy, vol. 88, no. 11, 2021, pp. 4021–4022.
14. Dufo-López, R., and J. L. Bernal-Agustin. "Multi-Objective Design of PV–Wind–Diesel–Hydrogen–Battery Systems." Renewable Energy, vol. 33, no. 12, 2018, pp. 2259–2272.
15. Luh, P. B., et al. "Grid Integration of Intermittent Wind Generation: A Markovian Approach." IEEE Transactions on Smart Grid, vol. 5, no. 2, Mar. 2018, pp. 732–741.
16. Di Somma, M., et al. "Operation Optimization of a Distributed Energy System Considering Energy Costs and Exergy Efficiency." Energy Conversion and Management, vol. 103, Oct. 2019, pp. 739–751.
17. Di Somma, M., et al. "Multi-Objective Operation Optimization of a Distributed Energy System for a Large-Scale Utility Customer." Applied Thermal Engineering, vol. 101, May 2023, pp. 752–761.
18. Yan, B., et al. "Exergy-Based Operation Optimization of a Distributed Energy System through the Energy-Supply Chain." Applied Thermal Engineering, vol. 101, May 2023, pp. 741–751.
19. Pruitt, K. A., R. J. Braun, and A. M. Newman. "Evaluating Shortfalls in Mixed-Integer Programming Approaches for the Optimal Design and Dispatch of Distributed Generation Systems." Applied Energy, vol. 102, Feb. 2021, pp. 386–398.
20. Katsigiannis, Y. A., P. S. Georgilakis, and E. S. Karapidakis. "Multiobjective Genetic Algorithm Solution to the Optimum Economic and Environmental Performance Problem of Small Autonomous Hybrid Power Systems with Renewables." IET Renewable Power Generation, vol. 4, no. 5, Sep. 2020, pp. 404–419.